Charge Ordering with Lattice Distortions in a Conductive MMX-Chain Complex, $Pt_2(dta)_4I$ ($dta = CH_3CS_2^-$)

Hiroshi Kitagawa,*,† Noriaki Onodera,† Takuya Sonoyama,† Masahiro Yamamoto,†,‡ Tadashi Fukawa,† Tadaoki Mitani,† Makoto Seto,§ and Yutaka Maeda§

Contribution from the Department of Physical Materials Science, the School of Materials Science, Japan Advanced Institute of Science & Technology, Tatsunokuchi, Ishikawa 923-1292, Japan, and Research Reactor Institute, Kyoto University, Kumatori, Sennan, Osaka 590-0494, Japan

Received May 12, 1999

Abstract: The charge-ordering states with lattice distortions of a halogen-bridged binuclear-metal mixed-valence complex (called MMX chain), $Pt_2(dta)_4I$ ($dta = CH_3CS_2^-$), have been investigated by transport, magnetic, and optical measurements. This complex is a binuclear unit-assembled conductor containing metal−metal bonds. It exhibits metallic conduction above room temperature, representing the first example of a metallic halogen-bridged one-dimensional transition-metal complex. Below 300 K it shows semiconducting behavior, which is considered to be of the Mott−Hubbard type due to electron correlation. The metal−semiconductor transition at 300 K ($= T_{M-S}$) is derived from a valence transition of Pt from an averaged-valence state of 2.5+ to a trapped-valence state of 2+ and 3+. The charge-ordering modes are considered to be $-I-Pt^{2+}-Pt^{3+}-I-Pt^{2+}-Pt^{3+}-I-Pt^{2+}-Pt^{3+}-I-Pt^{2+}-Pt^{3+}-I-$ for the semiconducting phase below T_{M-S} and $-I-Pt^{2.5+}-Pt^{2.5+}-I-Pt^{2.5+}-Pt^{2.5+}-I-Pt^{2.5+}-Pt^{2.5+}-I-Pt^{2.5+}-Pt^{2.5+}-I-$ for the metallic phase above T_{M-S}. ^{129}I Mössbauer spectroscopic study is reported for a low-temperature insulating phase below 80 K. The low-temperature electronic structure is considered to be an alternate charge-ordering state with lattice distortions of $-I-Pt^{2+}-Pt^{3+}-I-Pt^{3+}-Pt^{2+}-I-Pt^{2+}-Pt^{3+}-I-Pt^{3+}-Pt^{2+}-I-$. The present binuclear platinum complex inherently possesses valence instability of the intermediate valence 2.5+. X-ray photoelectron spectroscopy and polarized reflection measurements are also reported.

Introduction

Halogen-bridged one-dimensional (1-D) mononuclear-metal complexes, the so-called MX chain, provide a unique opportunity to investigate 1-D electronic systems.[1] Until now, more than 200 MX-chain materials have been synthesized. Thereby, many kinds of physical properties, derived from their one-dimensionality, have been observed, examples including intense and dichroic intervalence charge-transfer (IVCT) absorption,[2] progressive resonance Raman scattering,[3] luminescence with large Stokes shift,[4] midgap absorptions originating from solitons or polarons,[5] large third-order nonlinear optical properties,[6] charge-density wave (CDW) state,[7] Mott−Hubbard state with a large and antiferromagnetic coupling.[8] Since the photoexcited state of the MX chain shows unique optical properties, investigations have been focused, over the past 20 years, on their optical properties.

One of the most important features of the MX-chain materials is that their electronic states can be controlled by varying their

* To whom correspondence should be addressed. E-mail: hiroshi@jaist.ac.jp. FAX: +81(Japan)-761-51-1149.

† Japan Advanced Institute of Science and Technology.

‡ Japanese Patent Office.

§ Research Reactor Institute, Kyoto University (Mössbauer spectroscopic Measurements).

(1) (a) Robin, M. B.; Day, P. *Adv. Inorg. Chem. Radiochem*. **1967**, *10*, 247. (b) Allen. G. C.; Hush, N. S. *Prog. Inorg. Chem*. **1967**, *8*, 357. (c) Day, P. Low-Dimensional Cooperative Phenomena. In *Mixed Valence Chemistry and Metal Chain Compounds*; Keller, H. J., Ed.; Plenum Press: New York, 1974; p 191. (d) Keller, H. J., Ed. *Chemistry and Physics of One-Dimensional Metals*; Plenum Press: New York, 1977. (e) Day, P. The Physics and Chemistry of Low Dimensional Solids. In *Survey of Metal Chain Compounds*; Alcácer, L. Ed.; Reidel: Dordrecht, 1980; p 305. (f) Keller, H. J. Extended Linear Chain Compounds. In *Linear Chain Platinum Haloamines*; Miller, J. S., Ed.; Plenum Press: New York, 1982; Vol. 1, p 357. (g) Clark, R. J. H. Mixed-Valence Compounds. In *Electronic, Raman, and Resonance-Raman Spectroscopic Studies of Mixed-Valence Complexes*; Brown, D. E. Ed.; Reidel: Dordrecht, 1982; p 271. (h) Clark, R. J. H. *Adv. Infrared Raman Spectrosc*. **1983**, *111*, 95. (i) Mitani, T.; Inabe, T. Spectroscopy of New Materials. In *Spectroscopy of Proton and Electron Cooperation Systems*; Clark, R. J. H., Hester, R. E., Eds.; John Wiley & Sons: Chichester, 1993; p 291. (j) Yamashita, M. New Functional Materials. In *Synthetic Process and Control of Functionality Materials*; Tsuruta, T., Doyama, M., Seno, M., Eds.; Elsevier science: Tokyo, 1993; Vol. C, p 539. (k) Okamoto, H.; Yamashita, M. *Bull. Chem. Soc. Jpn*. **1998**, *71*, 2023.

(2) (a) Yamada, S.; Tsuchida, R. *Bull. Chem. Soc. Jpn*. **1956**, *29*, 894. (b) Wada, Y.; Mitani, T.; Yamashita, M.; Koda, T. *J. Phys. Soc. Jpn*. **1985**, *54*, 3143. (c) Okamoto, H.; Mitani, T.; Toriumi, K.; Yamashita, M. *Phys. Rev. B* **1990**, *42*, 10381.

(3) (a) Clark, R. J. H.; Franks, M.; Trumble, W. *Chem. Phys. Lett*. **1976**, *41*, 289. (b) Clark, R. J. H.; Kurmoo, M. *Inorg. Chem*. **1980**, *9*, 3522. (c) Tanino, H.; Kobayashi, K. *J. Phys. Soc. Jpn*. **1983**, *52*, 1446.

(4) (a) Tanino, H.; Nakahara, J.; Kobayashi, K.; *J. Phys. Soc. Jpn. Suppl*. **1980**, *49*, 695. (b) Tanaka, M.; Kurita, S.; Kojima, T.; Yamada, Y. *Chem. Phys*. **1985**, *96*, 343.

(5) (a) Matsushita, N.; Kojima, N.; Ban, T.; Tsujikawa, I. *J. Phys. Soc. Jpn*. **1987**, *56*, 3808. (b) Kuroda, N.; Sakai, M.; Nishina, Y.; Tanaka, S.; Kurita, S. *Phys. Rev. Lett*. **1987**, *58*, 2122. (c) Kurita, S.; Haruki, M.; Miyagawa, K. *J. Phys. Soc. Jpn*. **1988**, *57*, 1789. (d) Donohoe, R. J.; Ekberg, S. A.; Tait, C. D.; Swanson, B. I. *Solid State Commun*. **1989**, *71*, 49. (e) Okamoto, H.; Mitani, T.; Toriumi, K.; Yamashita, M. *Phys. Rev. Lett*. **1992**, *69*, 2248.

(6) Iwasa, Y.; Funatsu, E.; Hasegawa, T.; Koda, T. *Appl. Phys. Lett*. **1991**, *59*, 2219.

(7) (a) Whangbo, M.; Foshee, M. *Inorg. Chem*. **1981**, *20*, 113. (b) Gammel, G. T.; Saxena, A.; Batistic, I.; Bishop, A. R.; Phillpot, S. R. *Phys. Rev. B* **1992**, *45*, 6408. (c) Chakraverty, B. K. *J. Phys. (Paris) Lett*. **1979**, *40*, L99.

(8) (a) Nasu, K. *J. Phys. Soc. Jpn*. **1983**, *52*, 3865. (b) Nasu, K. *J. Phys. Soc. Jpn*. **1983**, *53*, 302. (c) Toriumi, K.; Wada, Y.; Mitani, T.; Bandow, S.; Yamashita, M.; Fujii, Y. *J. Am. Chem. Soc*. **1989**, *111*, 2341.

10.1021/ja9915910 CCC: $18.00
Published on Web 10/13/1999

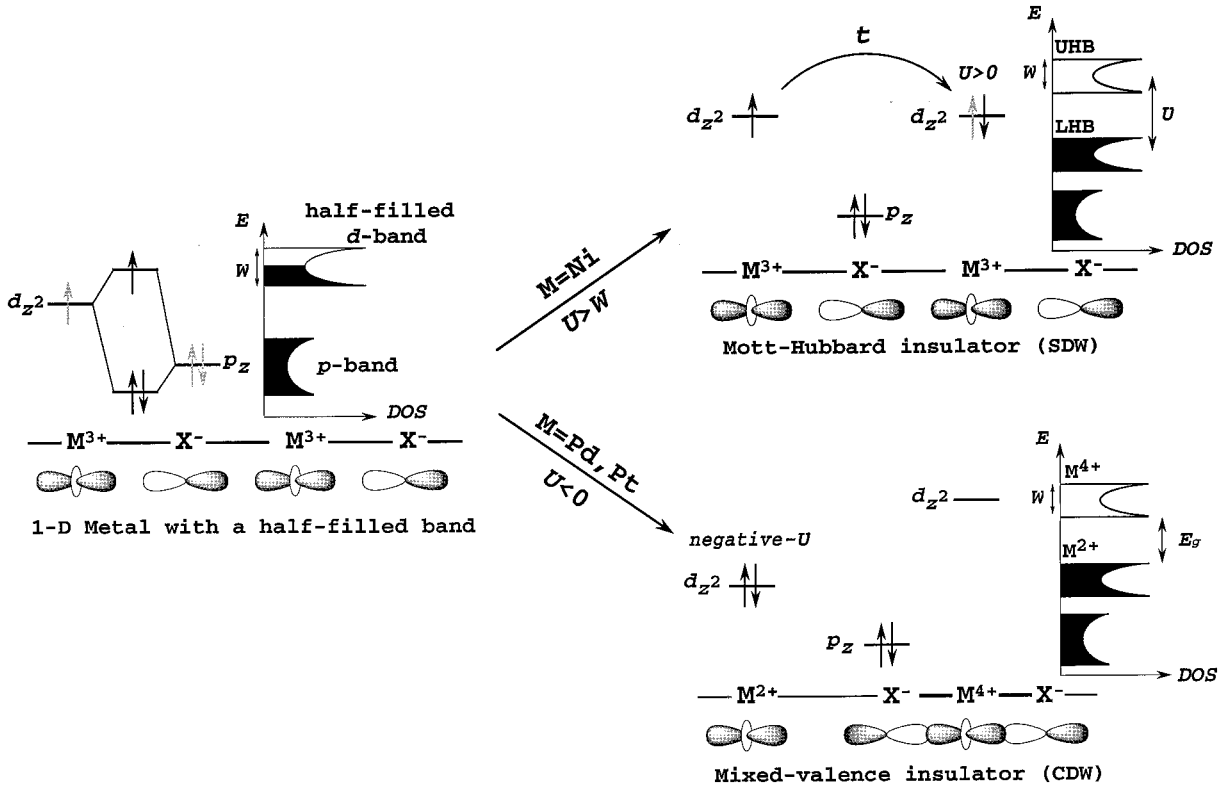

Figure 1. Schematic electronic structures for a 1-D metal with a half-filled d-band in the MX chain, a Mott−Hubbard insulator (SDW), and a mixed-valence insulator (CDW). UHB, LHB, and DOS abbreviate upper Hubbard band, lower Hubbard band, and density of states, respectively.

constituents of the transition metal ions, the bridging halogen ions, the terminal ligands, the counterions, and possibilities for intrachain or interchain hydrogen bonds, and also by external fields of light or pressure. In fact, the optical energy gap can be changed widely from 0.8 to 3.3 eV in MX-chain materials.[9] However, the control of energy gap in the lower-energy region near zero or equal to zero has not been attained. In such a system, a dynamical valence fluctuation of the metal ions is expected in the ground state.

As illustrated in Figure 1, if we imagine a hypothetical metallic chain with no Peierls distortion, the half-filled conduction band is made up primarily of an antibonding combination of transition metal M d_{z^2} orbitals and bridging halogen X p_z orbitals. In practice, MX chains with M = Ni are Mott−Hubbard or charge-transfer-type insulators (which is called the spin-density wave (SDW) by some physicists) due to strong on-site Coulomb repulsion (U).[8] On the other hand, MX chains with M = Pd, Pt are mixed-valence-type insulators (which is called the CDW) in which the charge disproportionation of the M into M^{2+} and M^{4+} cations of $\cdots M^{2+}\cdots X-M^{4+}-X\cdots$ occurs with lattice distortions and opens a gap at the Fermi energy due to the strong electron−lattice interaction, that is, negative-U effect.[7] Under high pressure, a pressure-induced metallization has been expected in MX chains. In general, the bandwidth (W) becomes wider, and the lattice distortion should be suppressed at high pressure. So the Mott−Hubbard-type or the mixed-valence-type insulator is often transformed to be a metallic or a semi-metallic state under high pressure. Extensive work on MX chains has been done,[10] in which the conductivity could be increased by as much as several orders of magnitude at high pressures, presumably because of the decreases in the Peierls distortion and band gap or an increase in the transfer energy ($t \approx W/4$) as pressure increased. However, up to now, no pressure-induced insulator-to-metal transition has yet been observed, except for 3-D MX-chain systems.[11]

Recently, attention has been directed to a MMX-chain system, $A_4[Pt_2(pop)_4X]\cdot nH_2O$ (A = Li, K, Cs, NH_4; *pop* = $H_2P_2O_5^{2-}$, diphosphonate; X = Cl, Br, I), in which the linear $-X-Pt_2(pop)_4-X-Pt_2(pop)_4-X-$ chain forms with a formal valence state for the metal ions of 2.5+. These binuclear Pt diphosphite complexes display interesting physical properties.[12] All of them are semiconductors or insulators with $\sigma \approx 10^{-2}-10^{-4}$ S·cm^{-1} for X = I, $10^{-3}-10^{-4}$ S·cm^{-1} for X = Br, and 10^{-7}S·cm^{-1} for X = Cl.

In the present work, we focus on another MMX-chain system of the title complex in which there exist 1-D $-I-Pt_2(dta)_4-I-Pt_2(dta)_4-I-$ (*dta* = $CH_3CS_2^-$, dithioacetate) chains, as shown in Figure 2. This material has a neutral-chain structure and a helical arrangement of four *dta*-ligand planes around the central Pt−Pt axis.[13] This was first synthesized and its basic properties studied by Bellitto et al.[13a] in 1982. Subsequently the Ni analogue was characterized by the same authors in 1985,[14a] and by NMR measurements.[14b,c] According to our

(9) Okamoto, H.; Mitani, T.; Toriumi, K.; Yamashita, *M. Mater. Sci. Eng.* **1992**, *B13*, L9.

(10) (a) Interrante, L. V.; Browall, K. W.; Bundy, F. P. *Inorg. Chem.* **1974**, *13*, 1158. (b) Interrante, L. V.; Bundy, F. P. *J. Inorg. Nucl. Chem.* **1977**, *39*, 1333. (c) Shirotani, I.; Kawamura, A.; Yamashita, M.; Toriumi, K.; Kawamura, H.; Yagi, T. *Synth. Met.* **1994**, *64*, 265. (d) Interrante, L. V. Low-Dimensional Cooperative Phenomena. In *Electron Transport in Some One-Dimensional Metal Complex Semiconductors*; Keller, H. J., Ed.; Plenum Press: New York, 1974; p 299. (e) Okamoto, H. unpublished work.

(11) (a) Kojima, N.; Kitagawa, H.; Ban, T.; Amita, F.; Nakahara, M. *Solid State Commun.* **1990**, *73*, 743. (b) Kitagawa, H.; Sato, H.; Kojima, N.; Kikegawa, T.; Shimomura, O. *Solid State Commun.* **1991**, *78*, 989. (c) Kitagawa, H.; Sato, H.; Kojima, N.; Kikegawa, T.; Shimomura, *Synth. Met.* **1991**, *41−43*, 1953. (d) Kojima, N.; Kitagawa, H.; Ban, T.; Amita, F.; Nakahara, M. *Synth. Met.* **1991**, *41−43*, 2347. (e) Kitagawa, H. *Systematic Studies on the Mixed-Valence States of Perovskite-Type Transition-Metal Complexes $Cs_2Au_2X_6$ (X = Cl, Br, I);* Ph.D. Thesis, Kyoto University, 1992. (f) Kitagawa, H.; Kojima. N.; Takahashi, H.; Môri, N. *Synth. Met.* **1993**, *55−57*, 1726. (g) Kojima, N.; Hasegawa, M.; Kitagawa, H.; Kikegawa, T.; Shimomura, *J. Am. Chem. Soc.* **1994**, *116*, 11368. (h) Kojima. N.; Fukuhara, F.; Kitagawa, H.; Takahashi, H.; Môri, N. *Synth. Met.* **1997**, *86*, 2175.

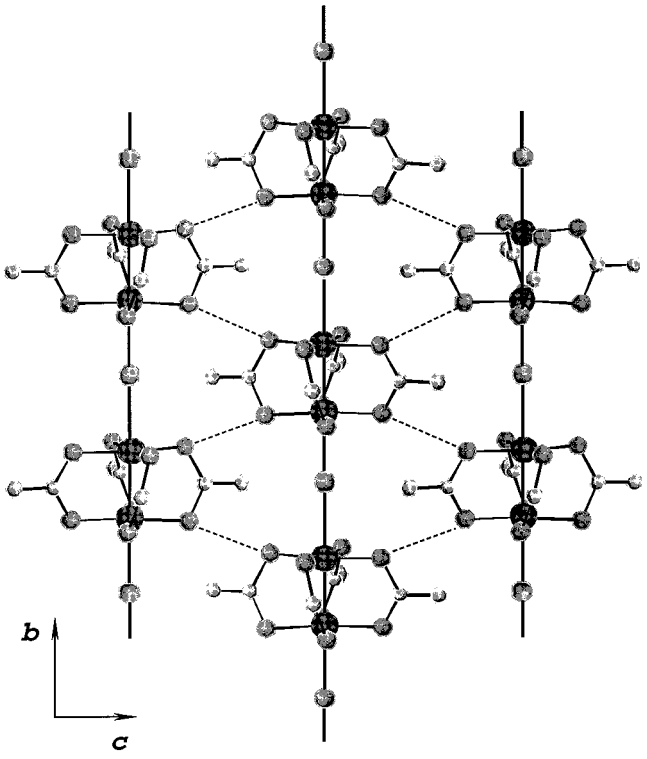

Figure 2. Crystal structure of $Pt_2(dta)_4I$ in the projection of the *bc* plane.[13] Dotted lines represent S···S van der Waals contacts along the *c* axis.

recent work,[15] the Pt salt was found to exhibit metallic conduction around room temperature (rt), which is the first observation of a metallic halogen-bridged 1-D transition-metal complex. Such a 1-D mixed-valence polynuclear unit-assembled conductor is expected to produce fluctuations in spin-charge-lattice coupling systems.

Before our results and discussions, we refer to the important features (a)−(d) of the MMX chain, compared with the MX chain.

(a) The formal oxidation state of the metal ions is 2.5+ (mixed valency of $M^{2+}(d^8) - M^{3+}(d^7)$) in MMX chains, while it is 3+ (mixed valency of $M^{2+}(d^8) - M^{4+}(d^6)$) in MX chains. So the difference between the oxidation states of metal ions becomes smaller in MMX chains. The trapped-valence state of $M^{2+}-M^{3+}$ in the MMX chain could possess an unpaired electron (a spin) per one dimer unit, although that of $M^{2+}-M^{4+}$ in the MX chain could not.

(b) Compared with the MX-chain system, the on-site Coulomb repulsion U is expected to be reduced due to the d_σ* character of the $M(d_{z^2})-M(d_{z^2})$ direct overlapping. This may contribute to high electrical conduction.

(c) As shown in Figure 2, owing to the ligands of *dta* containing S atoms and to the neutral-chain structure, weak S···S van der Waals contacts form between the chains,[13c] which may contribute to an increase of the dimensionality and suppression of the Peierls instability in this system.

(d) In a pure 1-D system, fluctuations such as spin, charge, and lattice originally play an essential role. In practice, those are often frozen due to weak interchain interactions. By making use of a polynuclear mixed-valence metal complex as building blocks, the internal degrees of freedom of 1-D electronic structure can be increased. In this sense, it is noteworthy that, very recently, a novel MMMMX-chain system, HH-$[Pt(2.5+)_4(NH_3)_8(\mu\text{-}C_4H_6NO)_4(Cl)](ClO_4)_3Cl_2$ was reported by Sakai et al.; there exists 1-D −Pt−Pt−Pt−Pt−Cl− infinite chain.[16]

In the present MMX chain, if the intrachain and the interchain interactions are controlled, it may be possible to revive the frozen fluctuations. Owing to its neutral chain structure, moreover, we might vary the band filling of this system by carrier doping.

From the interests mentioned so far, the physical properties in $Pt_2(dta)_4I$ were investigated by the X-ray photoelectron spectroscopy (XPS), electrical conductivity, thermoelectric power, polarized reflectance, polarized Raman spectroscopy, SQUID magnetometry, IR spectroscopy, and ^{129}I Mössbauer spectroscopy measurements.

Results and Discussion

1. Description of Possible Charge-Ordering Modes. The MMX chain is a binuclear unit-assembled system containing metal−metal bonds, so that there exists an internal degree of freedom of charge polarization in dimer units. Therefore, a wide variety of possible electronic structures is considered for the MMX system. Some of the possible 1-D charge-ordering states for the MMX chain are shown in Figure 3, with the electronic states of the MX chain. The valence numbers show formal oxidation states. Due to the orbital mixing between the metals through bridging X, the numbers should be expressed in the net charge. For example, $(2+\delta)+$ and $(4-\delta)+$ instead of 2+ and 4+ for the MX chain and $(2+\delta')+$ and $(3-\delta')+$ instead of 2+ and 3+ for the MMX chain, respectively ($0 \le \delta \le 1$, $0 \le \delta \le 0.5$). Schematic electronic structures for the MMX chain in the limit $U \rightarrow 0$ are also illustrated in Figure 4.

The modes (1) and (2) of the MMX chains have uniform charge distribution within the binuclear units, while modes (3) and (4) have charge polarization. The electron−lattice interaction in this system, which is originally derived from the nearest neighbor Coulombic attractive energy between the metal cation and the X anion, is expected to become stronger in the order of the mode (1) < (4) ≈ (3) < (2). In case of (2) and (3), the bridging halogens are expected to be deviated from the

(12) (a) Che, C. M.; Herbstein, F. H.; Schaefer, W. P.; Marsh, R. E.; Gray, H. B. *J. Am. Chem. Soc*. **1983**, *105*, 4606. (b) Stein, P.; Dickson, M. K.; Roundhill, D. M. *J. Am. Chem. Soc*. **1983**, *105*, 3489. (c) Kurmoo, M.; Clark, R. J. H. *Inorg. Chem*. **1985**, *24*, 4420. (d) Clark, R. J. H.; Kurmoo, M. *J. Chem. Soc., Dalton Trans*. **1985**, 579. (e) Clark, R. J. H.; Kurmoo, M.; Dawes, H. M.; Hursthouse, M. B. *Inorg. Chem*. **1986**, *25*, 409. (f) Butler, L. G.; Zietlow, M. H.; Che, C. M.; Schaefer, W. P.; Sridhar, S.; Grunthaner, P. J.; Swanson, B. I.; Clark, R. J. H.; Gray, H. B. *J. Am. Chem. Soc*. **1988**, *110*, 1155. (g) Swanson, B. I.; Stroud, M. A.; Conradson, S. D.; Zietlow, M. H. *Solid State Commun*. **1988**, *65*, 1405. (h) Jin, S.; Ito, T.; Toriumi, K.; Yamashita, M. *Acta Crystallogr. C* **1989**, *45*, 1415. (i) Stroud, M. A.; Drickamer, H. G.; Zietlow, M. H.; Gray, H. B.; Swanson, B. I. *J. Am. Chem. Soc*. **1989**, *111*, 66. (j) Yamashita, M. *Inorg. Chim. Acta* **1990**, *178*, 143. (k) Kimura, N.; Ohki, H.; Ikeda, R.; Yamashita, M. *Chem. Phys. Lett*. **1994**, *220*, 40. (l) Mitani, T.; Wada, Y.; Yamashita, M.; Toriumi, K.; Kobayashi, A.; Kobayashi, H. *Synth. Met*. **1994**, *64*, 291. (m) Wada, Y.; Furuta, T.; Yamashita, M.; Toriumi, K. *Synth. Met*. **1995**, *70*, 1195. (n) Yamashita, M.; Miya, S.; Kawashima, T.; Manabe, T.; Sonoyama, T.; Kitagawa, H.; Mitani, T.; Okamoto, H.; Ikeda, R. *J. Am. Chem. Soc*. **1999**, *121*, 2321.

(13) (a) Bellitto, C.; Flamini, A.; Gastaldi, L.; Scaramuzza, L. *Inorg. Chem*. **1983**, *22*, 444. (b) Yamashita, M.; Wada, Y.; Toriumi, K.; Mitani, T. *Mol. Cryst. Liq. Cryst*. **1992**, *216*, 207. (c) Kim, M.; Takata, K.; Ozawa, Y.; Toriumi, K., manuscript to be submitted. (d) Nakagami, S.; Kitagawa, H.; Yamamoto, M.; Sonoyama, T.; Morii, K.; Mitani, T., manuscript to be submitted.

(14) (a) Bellitto, C.; Dessy, G.; Fares, V. *Inorg. Chem*. **1985**, *24*, 2815. (b) Kinoshita, S.; Wakita, H.; Yamashita, M. *J. Chem. Soc., Dalton Trans*. **1989**, 2457. (c) Ikeda, R.; Kimura, N.; Ohki, H.; Furuta, T.; Yamashita, M. *Synthetic Metals* **1995**, *71*, 1907.

(15) (a) Kitagawa, H.; Onodera, N.; Ahn, J.-S.; Mitani, T.; Toriumi, K.; Yamashita, M. *Mol. Cryst. Liq. Cryst*. **1996**, *285*, 311. (b) Kitagawa, H.; Onodera, N.; Mitani, T.; Toriumi, K.; Yamashita, M. *Synth. Met*. **1997**, *86*, 193.

(16) Sakai, K.; Tanaka, Y.; Tsuchiya, Y.; Hirata, K.; Tsubomura, T.; Iijima, S.; Bhattacharjee, A. *J. Am. Chem. Soc*. **1998**, *120*, 8366.

MX chain

(1) Mott-Hubbard state

--X—[M^{3+}]—X—[M^{3+}]—X—[M^{3+}]—X—[M^{3+}]—X—[M^{3+}]—X--

(2) CDW state

--X—[M^{2+}]—X-[M^{4+}]-X—[M^{2+}]—X-[M^{4+}]-X—[M^{2+}]—X-[M^{4+}]-X--

MMX chain

(1) Averaged-valence state

--X—[$M^{2.5+}$-$M^{2.5+}$]—X—[$M^{2.5+}$-$M^{2.5+}$]—X—[$M^{2.5+}$-$M^{2.5+}$]—X--

(2) CDW state

--X—[M^{2+}-M^{2+}]—X-[M^{3+}-M^{3+}]-X—[M^{2+}-M^{2+}]—X-[M^{3+}-M^{3+}]-X--

(3) Charge-polarization state

--X—[M^{2+}-M^{3+}]-X—[M^{2+}-M^{3+}]-X—[M^{2+}-M^{3+}]-X—[M^{2+}-M^{3+}]-X--

(4) Alternate charge-polarization state

--X—[M^{2+}-M^{3+}]-X-[M^{3+}-M^{2+}]—X—[M^{2+}-M^{3+}]-X-[M^{3+}-M^{2+}]—X--

Figure 3. Some of the possible 1-D charge-ordering states for MX and MMX chains.

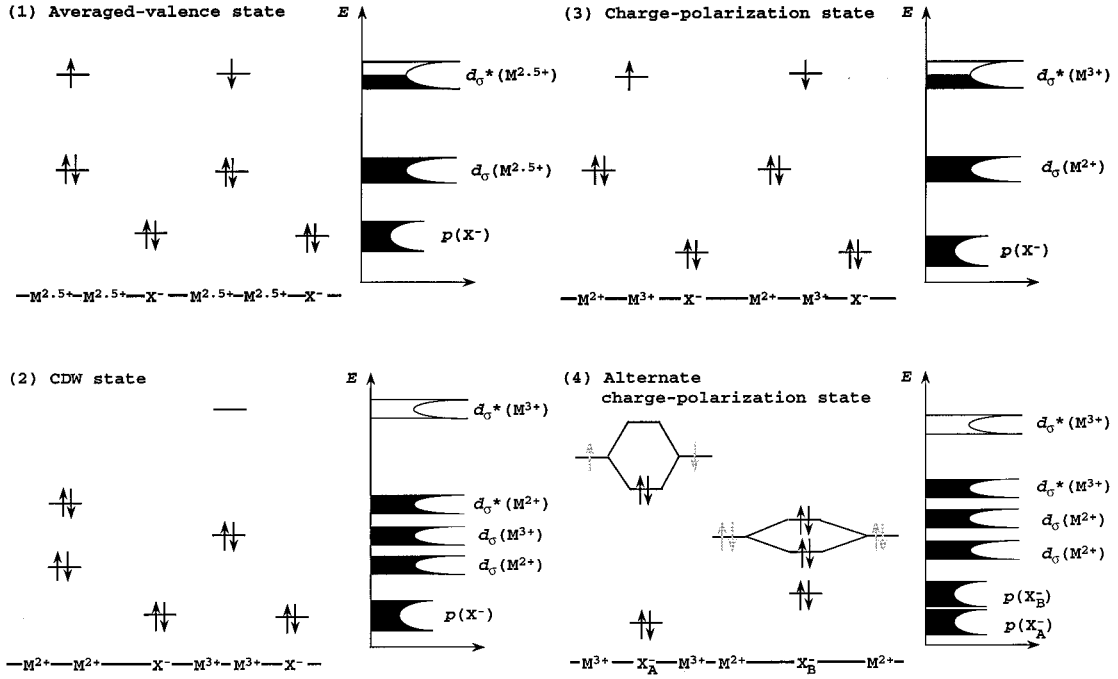

Figure 4. Schematic electronic structures for the MMX chain in the limit $U \rightarrow 0$; (1) Averaged-valence state, (2) CDW state, (3) Charge-polarization state, (4) Alternate charge-polarization state.

midpoints of two [$Pt_2(dta)_4$] dimers due to the electron−lattice interaction, analogous to that observed in the MX chain with M = Pt and X = I,[9] while those of (1) and (4) situated at the midpoints. The charge-ordering mode (1) with no lattice distortions is an averaged-valence state. In this case, each binuclear-metal unit possess an unpaired electron (a spin). An effectively half-filled conduction band, which is composed primarily of an antibonding combination of antibonding d_σ* orbitals of $M(d_{z^2})-M(d_{z^2})$ and $X(p_z)$ orbitals, is considered for the case of large overlapping of $M(d_{z^2})-M(d_{z^2})$ in the dimer. Two possible electronic states for the d_σ* conduction band are expected; a Mott−Hubbard insulator ($U > W \approx 4t$ in 1-D electronic system; W is bandwidth and t is transfer integral between dimers through the bridging $X(p_z)$ orbitals) and a 1-D metal ($W > U$). The mode (2) is a mixed-valence insulating (CDW) state where cell doubling occurs. In mode (3) where there exists an unpaired electron (a spin) at the Pt^{3+} site per one dimer unit, no cell doubling occurs, and therefore a Mott−Hubbard-type insulator or a 1-D Metal is expected. The possibility of mode (4) is of much interest because of its analogy to a spin-Peierls state which has not been observed for the MX chain. In this case the binuclear units, having one spin per unit, are dimerized, and this results in a 1-D alternate charge polarization. This state originates from spin-phonon interactions and nearest-neighbor interdimer Coulomb repulsion (V).[17]

(17) (a) Bray, J. W.; Interrante, L. V.; Jacobs, I. S.; Bonner, J. C. Extended Linear Chain Compounds. In *The Spin-Peierls Transition*; Miller, J. S., Ed.; Plenum Press: New York, 1982; Vol. 3, p 353. (b) Alcácer, L. Organic Conductors. In *Magnetic, ESR, NMR Properties*; Farges, J.-P., Ed.; Marcel Dekker: New York, 1994; p 269.

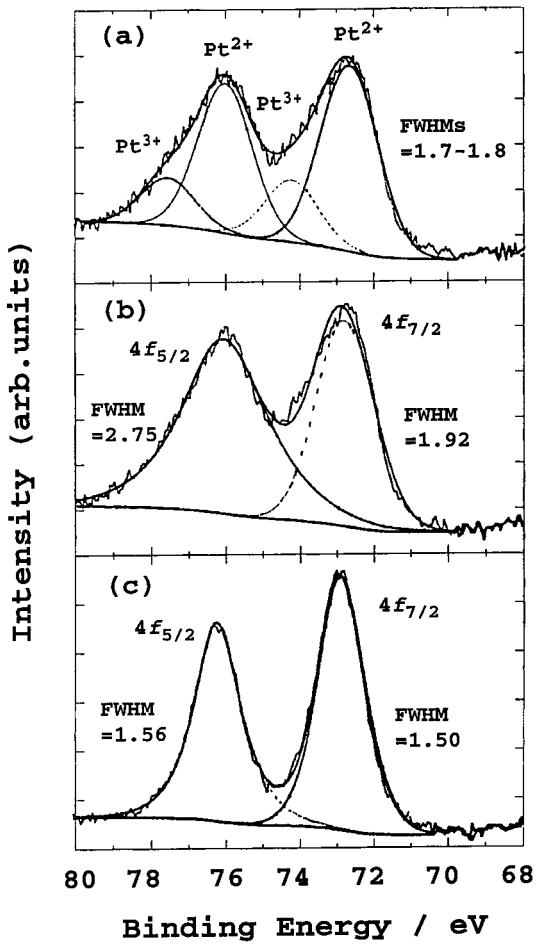

Figure 5. XPS spectra of Pt 4*f* region at rt; (a) a fit with two doublets for the observed spectrum of $Pt_2(dta)_4I$, (b) a fit with one doublet for the same spectrum of (a), (c) $Pt(H_2DAG)Cl_2$.

Table 1. Binding Energies (eV)[a] for the 4*f* Region of Platinum

	$4f_{5/2}$		$4f_{7/2}$	
complex	Pt^{2+}	Pt^{3+}	Pt^{2+}	Pt^{3+}
$Pt_2(dta)_4I$	76.0(1.77)	77.5(1.73)	72.7(1.81)	74.2(1.75)
$Pt(H_2DAG)Cl_2$	76.2(1.56)		72.9(1.50)	

[a] Values in parentheses correspond to the fwhm height for each peak.

2. Oxidation State. In general, the electron's transport of a molecule-based conductor is very sensitive to the oxidation state of molecule.[18] Therefore, the metal−semiconductor transition observed at 300 K may be expected to be related closely to dynamical valence fluctuation or static valence transition of Pt. To examine the valence state of Pt, XPS measurements were made on $Pt_2(dta)_4I$ in the temperature range 150−300 K. Figure 5 shows the XPS spectra of Pt 4*f* region for $Pt_2(dta)_4I$ and the Pt^{2+} control complex, $Pt(H_2DAG)_2Cl_2$ (H_2DAG = diaminoglyoxime). As shown in Figure 5b, the doublet is considerably broad, having fwhm's of 1.92 eV and 2.75 eV for $4f_{7/2}$ and $4f_{5/2}$, respectively, compared with the spectrum (Figure 5c) of the Pt^{2+} control complex (1.50 eV and 1.56 eV, respectively). The observed spectrum at rt was resolved into signals for Pt^{2+} and Pt^{3+} by using peak-decomposition software, as shown in Figure 5a; Binding energies of Pt 4*f* region given in Table 1 were all determined by a conventional deconvolution procedure. The binding energies of the doublet decomposed on the higher energy side are coincident with the average values[19] of binding energies for Pt^{2+} and Pt^{4+}. The intensity of the Pt^{3+} signal is smaller than that of Pt^{2+}, probably due to some decomposition (Pt^{3+} is partially reduced to Pt^{2+} by the X-ray beam despite of careful measurements). As previously reported by Bellitto et al.,[13a] XPS spectra of Pt in $Pt_2(dta)_4I$ at rt showed an averaged-valence state of 2.5+, which is in disagreement with our recent result. One of the reasons for this discordance may be attributable to the resolution of the XPS spectrometer. Most of the fwhm's observed for Pt single-valence complexes in our XPS system are ∼1.5 eV, compared with ∼2.0 eV observed in their system. No change of the XPS spectrum was observed at 150 K for the semiconducting state. It is noted that the mixed-valence complex $K_2Pt(CN)_4{\cdot}Br_{0.3}{\cdot}3.2H_2O$, which is a metallic molecule-based conductor and is therefore expected to have an averaged-valence state of $Pt^{2.3+}$, shows XPS spectra composed of two signals of Pt^{2+} and Pt^{4+},[20] because of a rapid time scale ($\sim 10^{-17}$ s) of the XPS experiment. It can be concluded that $Pt_2(dta)_4I$ exhibits mixed valency of Pt^{2+} and Pt^{3+} in the temperature range 150−300 K in the XPS time scale.

3. Transport Properties. Transport properties of this system can be related closely to the charge-ordering state of Pt. Electrical conductivity and thermoelectric power measurements were carried out. Figure 6a shows the temperature dependence of the electrical conductivity parallel to the chain axis (*b*) for the single crystal of $Pt_2(dta)_4I$. The rt conductivity is 13 $S{\cdot}cm^{-1}$, which is about 9 orders of magnitude higher than the typical value of a MX-chain complex. This complex shows a metal−semiconductor transition at 300 K (= T_{M-S}). Below 300 K, the compound is semiconducting but the behavior of the conduction is not simple activated type. A slight knee is observable around 230 K, which is related to be the anomalous negative temperature-dependence[13c,d] of the lattice constant *a*, mentioned below. Above T_{M-S}, it shows metallic conduction. The $Pt_2(dta)_4I$ complex is the second example, following KCP(Br),[21] of a transition-metal complex exhibiting metallic transport under ambient pressure without π-electronic system of ligands. Figure 6b shows the temperature dependence of the electrical resistivity parallel to the chain axis (*b*) in the temperature range of 50−380 K. Above 365 K, the resistivity decreases rapidly, which is considered to be derived from an order−disorder phase transition[13c] described below.

From single-crystal X-ray structure analyses for $Pt_2(dta)_4I$ by Toriumi et al.,[13c] it was revealed that an order−disorder phase transition occurs at 365 K from the low-temperature phase with space group *C*2/*c* to a high-temperature phase of *A*2/*m* in which the cell volume is half the low-temperature one. An endothermic peak was observed around 360 K on heating and a hysteresis in the differential-scanning-analysis (DSC) curve.[13c] The $Pt_2(dta)_4I$ complex has a helical arrangement of four *dta*-ligand planes around the central Pt−Pt axis. This helical structure of Pt dimers was found to be ordered in the low-temperature phase, while it was disordered in the high-temperature phase. The lattice parameter *a*, which is perpendicular to the chain axis, was found to exhibit an anomalous negative temperature dependence above 230 K. The observed slight knee of the conductivity is considered to relate to this negative temperature dependence of *a*.

(18) Cox, P. A.; Egdell, R. G.; Orchard, A. F. Mixed-Valence Compounds. In *Photoelectron Spectroscopy of Mixed-Valence Compounds*; Brown, D. E., Ed.; Reidel: Dordrecht, 1982; p 475.

(19) Handbook of X-ray Photoelectron Spectroscopy, Perkin-Elmer.

(20) Sawatzky, G. A.; Antovides, E. *J. Phys. (Paris) C* **1976**, *4* 117.

(21) (a) Krogmann, K.; Hausen, H. D. *Z. Anorg. Allg. Chem.* **1968**, *358*, 67. (b) Zeller, H. R. *J. Phys. Chem. Solids* **1974**, *35*, 77. (c) Heger, G.; Deiseroth, H. J.; Schultz, H. *Acta Crystallogr. B* **1978**, *34*, 725.

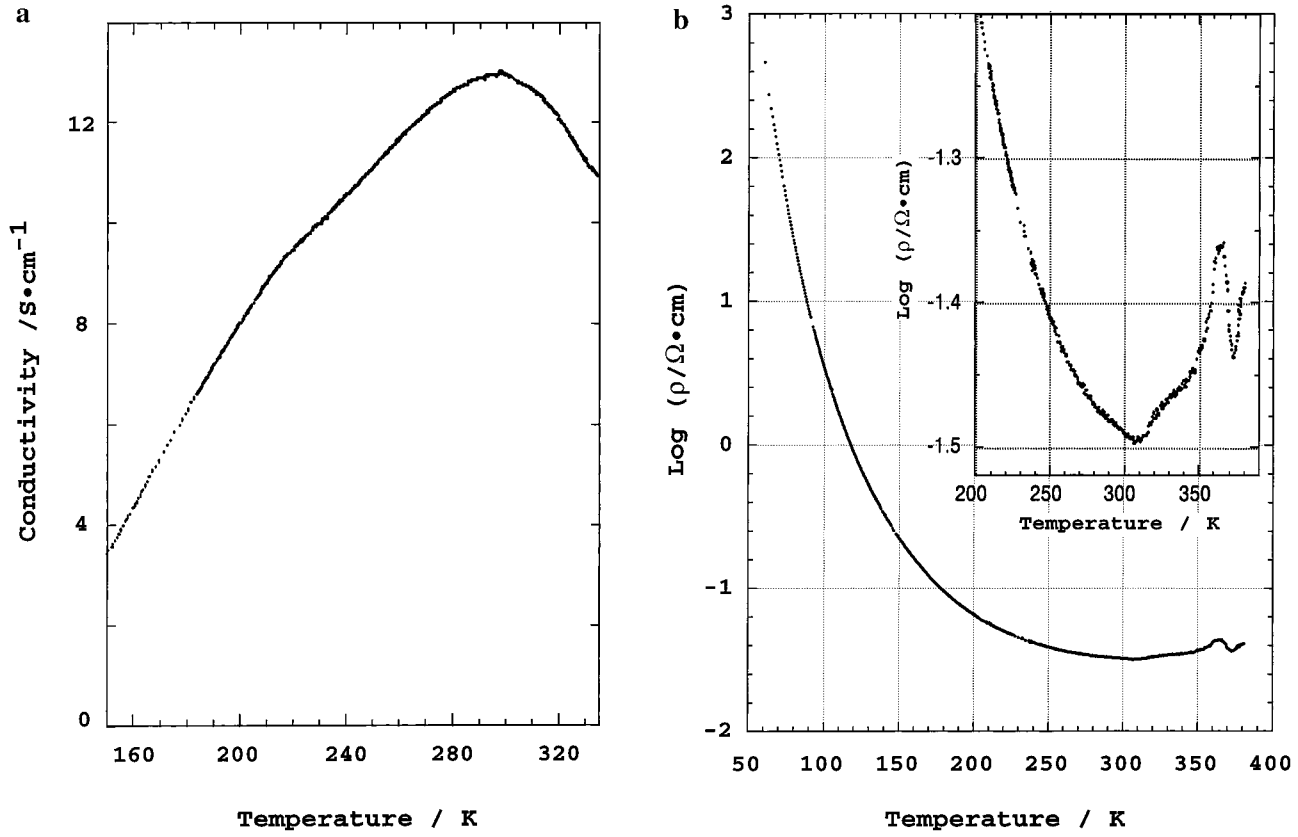

Figure 6. (a) Temperature dependence of the electrical conductivity of a single-crystal $Pt_2(dta)_4I$ parallel to the chain axis *b* in the temperature range of 150−335 K. (b) Temperature dependence of the electrical resistivity of a single-crystal $Pt_2(dta)_4I$ parallel to the chain axis *b* in the temperature range of 50−380 K, measured for different crystal and with different transport equipment, from (a). The inset is the magnification of high-temperature parts.

As shown in Figure 6b, this phase transition begins at 365 K and is completed at 375 K. The resistance drop at 365 K implies that the resistivity in high-temperature phase is smaller than that in low-temperature phase. The temperature dependence above 375 K shows that the high-temperature disordered phase is also metallic.

Bellitto et al.[13a] and Yamashita et al.[13b] reported that this salt was not a metal but a semiconductor, which is not consistent with our result. This disagreement is considered to be due to the difference of experimental methods. Prior conductivity measurements were performed on compressed polycrystalline samples with a four-probe method or single crystals with a two-probe one. On the other hand, Shirotani et al.[10c] reported that the electrical conduction of the evaporated thin film of $Pt_2(dta)_4I$ was semiconducting with an activation energy of 0.04 eV below 360 K. They also observed similar resistance drop above 365 K for the evaporated thin film,[10c] which is supposed to be due to the order−disorder phase transition.

Thermoelectric power measurement has been frequently used for molecular conductors as a conventional method of the estimation of transport properties because of its low sensitivity to microcracks within crystals. The result of the thermoelectric power *S* as the function of the temperature in $Pt_2(dta)_4I$ is shown in Figure 7. The metal−semiconductor and the metal−metal transitions were also confirmed by the temperature dependence of *S*. When $T < 300$ K, the sign of the thermoelectric power changes from negative values to positive ones with cooling. As the temperature is increased above 300 K, the negative *S* values decrease slowly with a slight kink around 360 K, and then are almost temperature-independent above 385 K. The divergent increase below 300 K is indicative of opening gap at the Fermi energy: The loss of the free carriers is accompanied by a sharp increase of *S*, according to Bolzmann theory for the semicon-

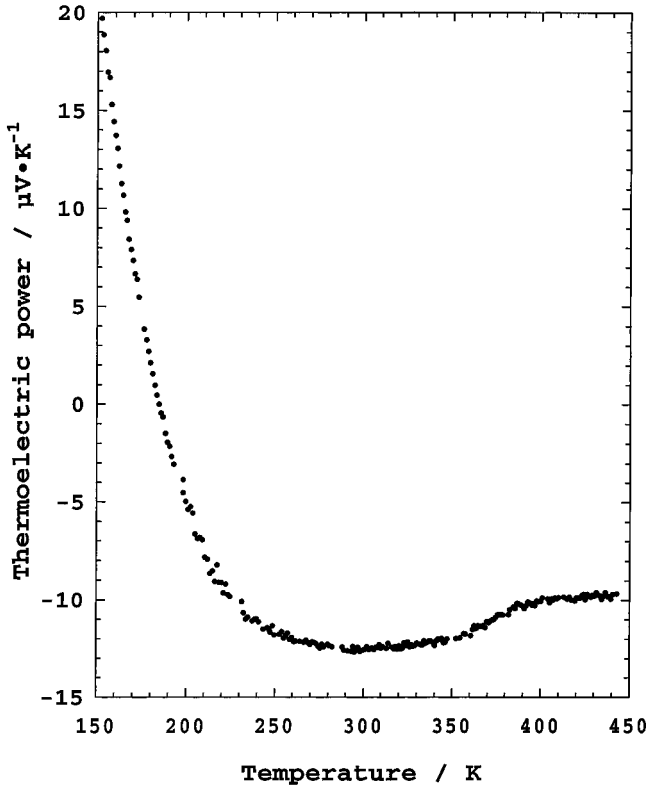

Figure 7. Temperature dependence of the thermoelectric power of a single-crystal $Pt_2(dta)_4I$ parallel to the chain axis *b*.

ducting state[22]

$$S = -(k_B/|e|)[\{(b-1)/(b+1)\}(E_g/2k_BT) + (^3/_4)\ln(m_h/m_e)] + \text{constant} \quad (1)$$

where k_B denotes the Boltzmann's constant, e the electronic charge of carriers, b the ratio of electron to hole mobility, E_g the band-gap energy, and m_h and m_e the effective mass of the holes and electrons, respectively. The thermoelectric power result confirms the conclusion of the conductivity measurements that the $Pt_2(dta)_4I$ complex undergoes a metal−semiconductor transition at 300 K. The sign of S in the semiconducting state depends on the ratio of b and the impurity content in the energy gap. The slight kink at 360 K is related to the beginning of the order−disorder phase transition to higher-temperature phase, and the temperature of 385 K, to the ending of the transition. Slight differences in transition temperatures between σ and S measurements are due to the different transport equipment.

Since the thermoelectric power of 1-D metals usually shows linear temperature dependence, it has been often applied for the estimation of the bandwidth. If we neglect electronic effects for the diffusion thermoelectric power and assume a single particle approach for a 1-D free electron gas, i.e., a tight-binding approach,[22]

$$S = -(2\pi^2k_B{}^2T/3|e|W)[\cos(\pi\rho/2)/\sin^2(\pi\rho/2)] \quad (2)$$

where W denotes the bandwidth ($\sim 4t$) and ρ the degree of bandfilling ($\rho = 1$ means a half filling). If the 1-D system were composed of a half-filled conduction band, however, S would exhibit zero or a small value and would be temperature-independent because of $\cos(\pi\rho/2) \approx 0$, and then W could not be estimated from the slope of $S(T)$.

The temperature-independent S behavior was observed above 385 K for $Pt_2(dta)_4I$. In the present system, the 1-D d_{z^2} band is originally three-quarters-filled: $(5d_{z^2})^2(5d_{z^2})^1$, if the intradimer transfer $t_{intra} \approx 0$. When the t_{intra} is not so small, the three-quarters-filled band is partially split into bands of d_σ and d_σ*. In this case, the d_{z^2} band becomes effectively half-filled: $(d_\sigma^*)^1$ at the Fermi energy. The overlapping of d_{z^2} orbitals in the dimer is expected to be large because of the quite short intermetallic Pt−Pt distance (2.68 Å).[13] The observed temperature-independent S behavior can be understood by the effectively half-filled band composed primarily of an antibonding combination of $(5d_\sigma^*)^1$ of the binuclear unit and $(5p_z)^2$ of bridging iodide ion. Between 300 and 360 K, S is almost temperature-independent with a small value, which is also indicative of a metal of $\rho \sim 1$.

4. Reflectivity Properties. Highly conductive molecular solids show anisotropic metal-like reflectance associated with intermolecular charge transfer in the IR region.[23] Although an electron gas giving the plasma edge does not occur in molecular metals, a quasi-free transport of electrons exhibits metallic properties in the near-IR region. To investigate metallic properties of this system, polarized reflectivity spectra of a single-crystal $Pt_2(dta)_4I$ were measured at rt As shown in Figure 8, though this system possesses S···S contacts between the 1-D chains, no prominent structure was observed in the energy region from 0.5 eV to 3.5 eV for the polarization perpendicular to the chain axis ($E \perp b$). On the other hand, for the polarization parallel to the chain axis ($E \parallel b$), high reflectivity was observed, which is consistent with the conductive transport of electrons along the 1-D axis mentioned above. Anisotropy of the reflection shows that $Pt_2(dta)_4I$ has a 1-D electronic structure. This implies that atomic orbitals of sulfur do not contribute to the conduction bands, which is different from BEDT-TTF-based 2-D conductors.[24] It should be noted that, in contrast to $Pt_2(dta)_4I$, the polarized reflectance spectrum of $Ni_2(dta)_4I$ has a sharp peak at 0.6 eV parallel to the chain axis, which is consistent with its semiconducting behavior of a Mott−Hubbard insulator.[13b,25]

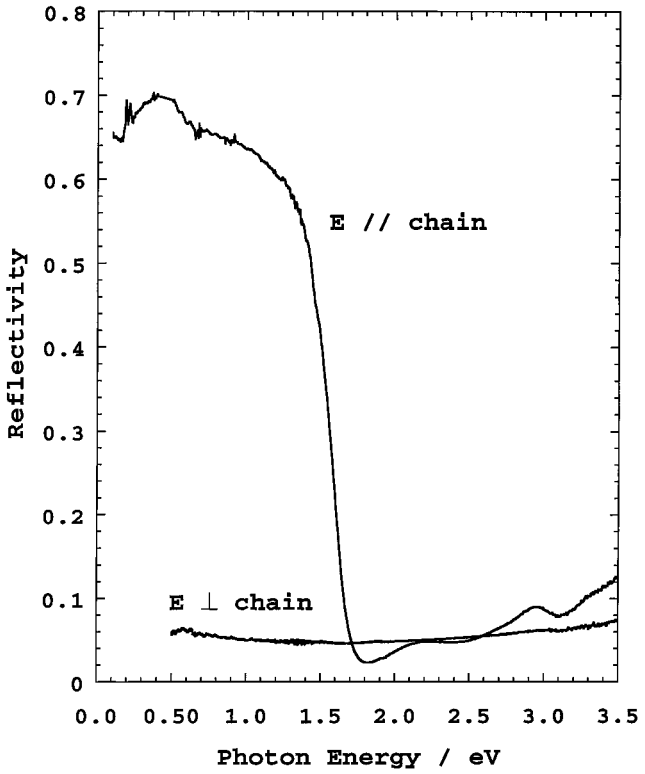

Figure 8. Polarized reflectivity spectra of a single crystal parallel and perpendicular to the chain axis, b at rt

Figure 9 shows the optical conductivity of $Pt_2(dta)_4I$ as obtained from Kramers−Kronig analysis[23,24,26] of polarized reflectivity data. This seems to exhibit non-Drude features at low frequencies. The rt conductivity of $Pt_2(dta)_4I$ is not so high ($13\ S\cdot cm^{-1}$), and it seems that the far-infrared conductivity extrapolated to 0 eV matches this value well, although it needs to measure the far-infrared region. For the chain axis component, the dominant absorption features are a strong band centered at 0.3 eV and two bands at 2.2 eV and 2.9 eV. The bands of 2.2 eV and 2.9 eV are considered to be attributable to the ligand-to-metal charge-transfer (LMCT; $I(p_\sigma) \rightarrow Pt(d_\sigma^*)$) and the intradimer ($d_\pi^* \rightarrow d_\sigma^*$) transitions, respectively; The two bands are also observed for oxidized $Pt_2(dta)_4I_2$ of which the d_σ* orbital is unoccupied, and both are not observed for the reduced species $Pt_2(dta)_4$ when d_σ* is fully occupied.[13a,27] The former band is

(22) Chaikin, P. M. The Physics and Chemistry of Low Dimensional Solids. In *Transport in Quasi-One-Dimensional Solids*; Alcácer, L., Ed.; Reidel: Dordrecht, 1980; p 53.

(23) (a) Jacobsen, C. S. Highly Conducting Quasi-One-Dimensional Organic Crystals. In *Optical* Properties; Conwell, E. Ed.; Semiconductors and Semimetals, Academic Press: San Diego, 1988; Vol. 27, p 293. (b) Graja, A. Organic Conductors. In *Optical Properties*; Farges, J.-P., Ed.; Marcel Dekker: New York, 1994; p 229.

(24) Williams, J. M.; Ferraro, J. R.; Thorn, R. J.; Carlson, K. D.; Geiser, U.; Wang, H. H.; Kini, A. M.; Whangbo, M.-H. Organic Superconductors. In *Polarized Reflectance in the Infrared*; Prentice Hall: New Jersey, 1992; p 229 and references therein.

(25) Wada, Y.; Yamashita, M. *Proceedings of the First International Conference on Intelligent Materials*, Kanagawa, 1992; p 147.

(26) Kuzmany, H. *Solid State Spectroscopy*; Springer: Berlin, 1998; pp 101−120.

(27) (a) Bellitto, C.; Flamini, A.; Piovesana, O.; Zanazzi, P. F. *Inorg. Chem.* **1980**, *19*, 3632. (b) Onodera, N.; Kitagawa, H.; Mitani, T., unpublished work.

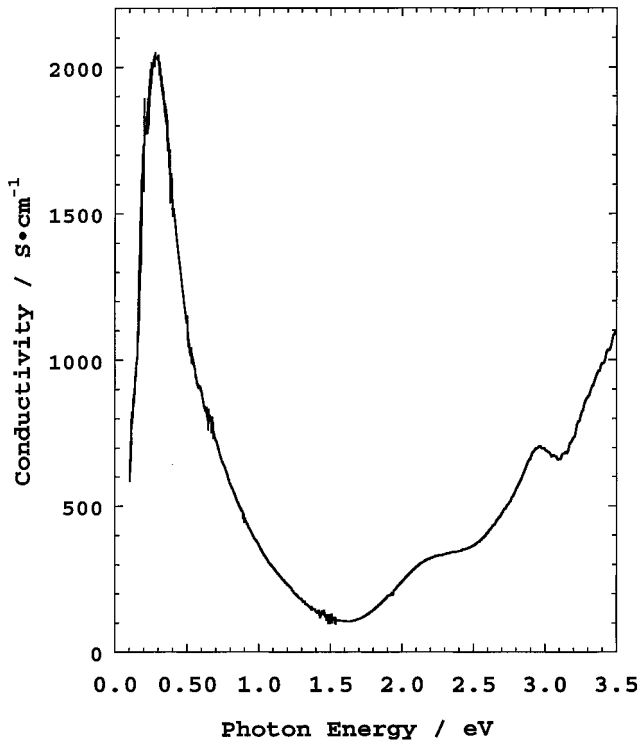

Figure 9. Optical conductivity (*E*//chain) obtained by the Kramers−Kronig analysis of the measured reflectivity at rt

shifted to higher-energy side in the order of $Pt_2(dta)_4I_2$ (2.2 eV) < $Pt_2(dta)_4Br_2$ (2.5 eV) < $Pt_2(dta)_4Cl_2$ (2.7 eV), while the energy of the latter band is almost unchanged.[13a] These facts are consistent with the above assignments. The strong band at 0.3 eV should be associated with interdimer charge transfer from the electronic configuration of $d_\sigma^2 d_\sigma^{*1}$, $d_\sigma^2 d_\sigma^{*1}$ to that of d_σ^2, $d_\sigma^2 d_\sigma^{*2}$.

As is well known in molecular conductors, the lower the dc conductivity, the higher is the frequency around which the oscillator strength is centered.[23] Most of the organic Mott-insulators having half-filled bands display a pronounced broad maximum around 1 eV, which is roughly understood as $U - V$ in the limit $t \rightarrow 0$. For more conducting molecular solids, on the other hand, the optical conductivity typically peaks around 0.3 eV, which is considered to be attributed to a continuous transition to a $2k_F$ or $4k_F$ fluctuating Peierls system.[23] The observed strong band at 0.3 eV for $Pt_2(dta)_4I$ could be basically explained as well. For the $Pt_2(C_2H_7CS_2)_4I$, similar optical conductivity band was observed at 0.3 eV. It is noted that the sharpness of the band strongly depends on temperature, but its position is relatively temperature independent.[28] It could be imagined from these results, that fluctuations play an important role in the present system.

5. Polarized Raman Spectra. Raman spectroscopy has been used widely to study the vibrational and structural properties of MX-chain or MMX-chain compounds, since Raman modes are very sensitive to the symmetry of the metal-complex unit and its translational geometry.[29] Some of the possible 1-D charge-lattice ordering modes for the −Pt−Pt−I− chain are shown in Figure 3. In the case of mode(1) or (4), where the Pt−Pt distances of the $[Pt_2(dta)_4]$ dimer units are uniform, the Pt−Pt stretching mode, ν(Pt−Pt), would be a singlet. In addition,

(28) Kitagawa, H.; Fukawa, T.; Mitsumi, M.; Toriumi, K. *J. Am. Chem. Soc.*, manuscript to be submitted.

(29) (a) Clark, R. J. H. *Infrared Raman Spectrosc.* **1984**, *11*, 95. (b) Clark, R. J. H.; Walton, J. R. *Inorg. Chem. Acta* **1987**, *129*, 163.

Table 2. Wavenumbers (cm^{-1}) and Assignments of Bands Observed for $Pt_2(dta)_4I$ and the Control Complexes

complex	ν(MM)	ν(MX)	δ(SMS)	δ(MSC)	ν(MS)	δ(SCS)	ν(CS)
$Pt_2(dta)_4I$	64 s	115 vw	164 s	247 m	267 vs	441 m	603 m
$Pt_2(dta)_4$	74 w		147 vw	246 m	270 m	441 vw	605 m
$Pt_2(dta)_4I_2$	64 m	115 vs	210 m	250 w	268 m	443 m	611 m
$Pt_2(dta)_4Br_2$	76 w	147 vs	220 w	252 w	271 w	441 w	610 vw
$Pt_2(dta)_4Cl_2$	77 w	184 s		252 m	271 m	444 vw	610 vw
$Ni_2(dta)_4I$	94 w			210 vw	240 m	420 vw	610 w

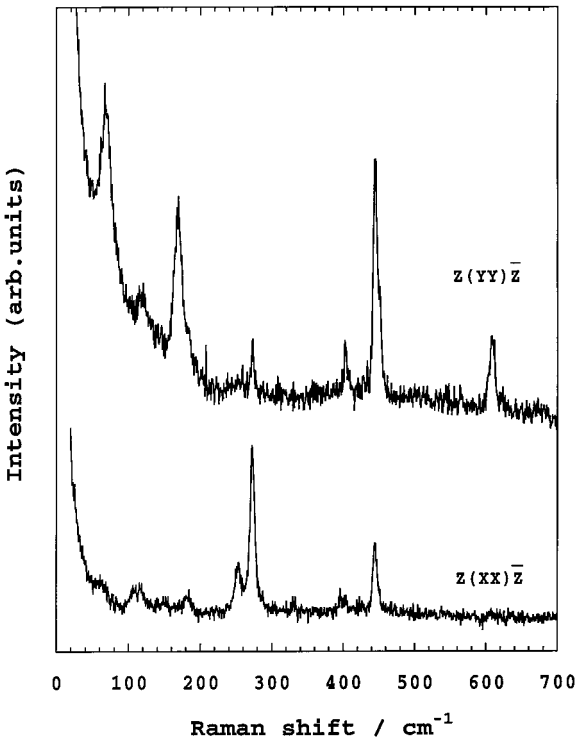

Figure 10. Raman spectra of a single-crystal $Pt_2(dta)_4I$ at rt for the polarizations of Z(YY)$\bar{Z}$ and Z(XX)$\bar{Z}$.

if the iodine ions were centrally placed between the $[Pt_2(dta)_4]$ dimer units, the symmetric Pt−I stretching mode, ν(Pt−I), would be Raman-inactive. In the case of (3) where the Pt−Pt distances are also uniform, the ν(Pt−Pt) mode would be a singlet but the ν(Pt−I) mode would be Raman-active. In the case of (2) where the Pt−Pt distances are different from one another, the ν(Pt−Pt) mode would be a doublet and the ν(Pt−I) mode would be allowed. Accordingly, it seemed important to investigate the Raman spectra of this mixed-valence complex.

Wavenumbers and assignments of bands observed in the Raman spectra of $Pt_2(dta)_4I$ and the control complexes are listed in Table 2. Figure 10 shows the Raman spectra of $Pt_2(dta)_4I$ just above T_{M-S} for the incident-laser polarizations parallel to the *b** and *c** axes. Very weak ν(Pt−I) mode at 115 cm^{-1} and no overtones were observed for the polarization of Z(YY)$\bar{Z}$ in $Pt_2(dta)_4I$. From these results, an important conclusion is drawn, i.e., that iodine ions can be centrally bridging between the $Pt_2(dta)_4$ units, otherwise the ν(Pt−I) mode would be strongly Raman-active. This is in good agreement with the results of X-ray single-crystal analyses.[13] On the contrary, the strong ν(Pt-X) mode (X = Cl, Br, I) and the overtones were observed for another MMX-chain system, $K_4[Pt_2(pop)_4X]\cdot nH_2O$, in which the bridging halogen ions deviate from the midpoints of $[Pt_2(pop)_4]^{3-}$ units.[12b−d,f,g,i] The wavenumber of the ν(Pt−I) mode of $Pt_2(dta)_4I$ (115 cm^{-1}) is much lower than each of $[Pt_2(pop)_4I_2]^{4-}$ (189 cm^{-1}) and $[Pt_2(pop)_4I]^{4-}$ (185 cm^{-1}),[12c] and equal to the discrete species $Pt_2(dta)_4I_2$ (115 cm^{-1}). The other

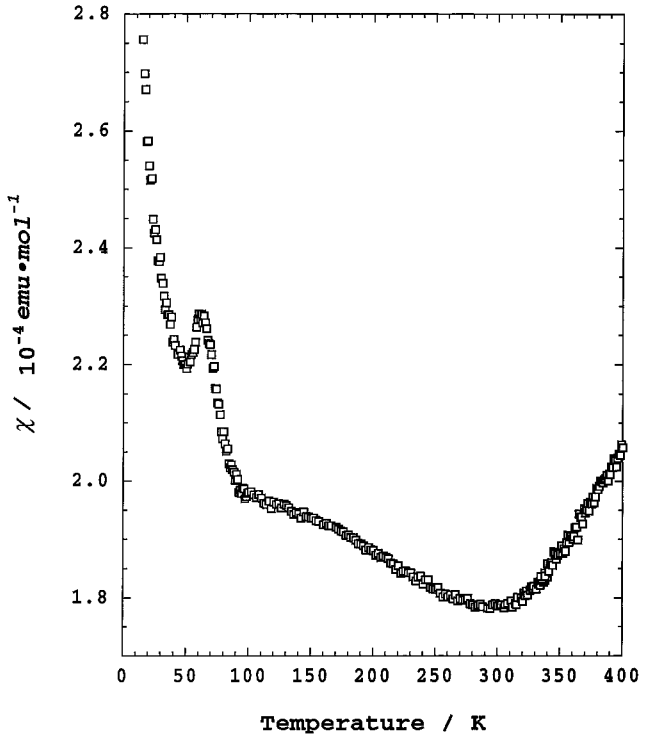

Figure 11. Temperature dependence of the magnetic susceptibility of $Pt_2(dta)_4I$; the data are corrected for the ligand and metal core diamagnetic contributions.

important mode, which is assigned to Pt−Pt stretching mode (64 cm^{-1}), is a singlet. So the chain structure of the metallic state can be interpreted in terms of either model of the mode (1) or (4) from the Raman study. The ν(Pt−Pt) and ν(Pt−I) modes are strongly y-polarized, which reflects a 1-D electron−lattice coupled system. The temperature dependence of Raman spectra is expected to provide useful information on low-temperature structural mode, and its measurements is being planned.

6. Magnetic Properties. To clarify the origin of the metal−semiconductor transition observed at 300 K, the temperature dependence of magnetic susceptibility was measured, as shown in Figure 11. The data were corrected for the ligand and metal core diamagnetic contributions [$= -4.07 \times 10^{-4}$(emu/mol)] which represents the sum of the value measured for nonmagnetic $Pt_2(dta)_4$ and half the reference value of I_2. In the metallic region of $300 < T < 400$ K, the susceptibility decreases with temperature on the order of 20%, which has been often observed in 1-D molecular conductors. In most of 1-D molecule-based conductors, the temperature dependence of the susceptibility deviates considerably from the Pauli temperature-independent paramagnetism. Many explanations have been given to account for the deviations from the expected enhanced-Pauli χ_s in the metallic regime.[30] Since the Hubbard model is solved both for the weak-coupling limit ($t \gg U, V$) and the strong-coupling limit ($U, V \gg t$) but not for the intermediate value of $U/4t$, quantitative agreement was neither expected nor obtained. However, we believe that one of the most important effect to deviations to the Pauli-like susceptibility in $Pt_2(dta)_4I$ is the following. If the Coulomb interactions are important, χ_s will deviate toward Bonner−Fisher behavior[31] due to exchange interactions. As mentioned afterward, the Coulomb interactions play an important role in the MMX-chain system, that is, the Mott−Hubbard system with $U \approx 4t$.

Below the metal−semiconductor transition, on the other hand, the magnetic susceptibility increases slightly with a slight convex in the χ_s-T curve upon cooling to 90 K. If a transition relates to Peierls (CDW) instability, the (spin) susceptibility should be activated below the transition because of the freezing of both charge and spin degrees of freedom. The opposite behavior was observed below 300 K in the susceptibility data. The MMX-chain system is strongly suggested by thermoelectric power measurements to be an electronic system having a effectively half-filled conduction band. The most important effect especially for the 1-D half-filled system is electron−electron Coulomb interactions of U and V. Since only the charge degree of freedom is lost while the spin degree of freedom is maintained below T_{M-S}, the semiconducting state can be considered to be a $4k_F$ CDW, that is a Mott−Hubbard insulator in a half-filled band with magnetic disorder and often lead to a SDW or spin-Peierls ground state at low temperatures. Such the Mott−Hubbard transition usually shows no obvious anomaly in χ_s since it is a crossover-type transition from the itinerant-electron (Pauli) paramagnetism to localized paramagnetism.[32] In case of a Mott−Hubbard transition the translational symmetry of the binuclear unit is maintained. So either of charge-ordering mode (1) or (3) can be the semiconducting state just below T_{M-S}. The susceptibility increases rather rapidly below 90 K, decreases between 60 and 50 K, increases again down to 20 K, and then increases rapidly to 4.2 K due to a small amount of paramagnetic impurities. There seem to be several transitions below 90 K. Very recently, several anomalies were found out by ^{1}H NMR measurements.[33]

7. Valence Transition. Detailed information on the electronic structure can be also obtained from IR study. For example in a report by Okaniwa et al.,[34] the splitting of the N−H stretching mode in *chxn* ligands for M = Pt or Pd of $[M(chxn)_2Br]Br_2$ (*chxn* = 1*R*, 2*R*-diaminocyclohexane) shows a good correlation with the amplitude (δ) of the CDW state in the ···Br−$M^{(3-\delta)+}$−Br−$M^{(3+\delta)+}$−Br−$M^{(3-\delta)+}$−Br− $M^{(3+\delta)+}$−Br··· chain, i.e., with the deviation of the bridging halogen ion from the midpoint of M ions; however for the M = Ni, no splitting of the mode was observed, which is consistent with the Mott−Hubbard state (the single-valence state, ···Br−Ni^{3+}−Br−Ni^{3+}−Br−Ni^{3+}−Br−Ni^{3+}−Br···). Thus the IR stretching mode of the ligand is a very sensitive and useful probe to the oxidation state of the metal. Therefore, we have focused on the C═S stretching mode in *dta* ligands of $Pt_2(dta)_4I$ in the temperature range from 11 to 475 K.

As shown in Figure 12, the C═S stretching mode at 1180 cm^{-1} was split into two bands below T_{M-S}. The IR mode of the CS_2 stretching vibration is considered to be quite sensitive and reflects the charge distribution of the intermetallic Pt−Pt bond in the $[Pt_2(dta)_4]$ dimer unit. The single peak observed above T_{M-S} strongly suggests that the electronic state is in the uniform charge distribution, that is mode (1). On the other hand, the two peaks observed below T_{M-S} show a trapped-valence state of Pt^{2+} and Pt^{3+}. This is evidence of a valence transition from an averaged-valence state to a trapped-valence state at

(30) Scott, J. C. Highly Conducting Quasi-One-Dimensional Organic Crystals. In *Magnetic Properties*; Conwell, E. Ed.; Semiconductors and Semimetals, Academic Press: San Diego, 1988; Vol. 27, p 386 and references therein.

(31) Bonner, J. C.; Fisher, M. E. *Phys. Rev. A* **1964**, *135*, 640.

(32) (a) Iwasa, Y.; Mizuhashi, K.; Koda, T.; Tokura, Y.; Saito, G. *Phys. Rev. B* **1994**, *49*, 3580. (b) Mori, T.; Kawamoto, T.; Yamaura, J.; Enoki, T.; Misaki, Y.; Yamabe, T.; Mori, H.; Tanaka, S. *Phys. Rev. Lett.* **1997**, *79*, 1702.

(33) Takefuji, S.; Kanoda, K., manuscript to be submitted.

(34) Okaniwa, K.; Okamoto, H.; Mitani, T.; Toriumi, K.; Yamashita, M. *J. Phys. Soc. Jpn.* **1991**, *60*, 997.

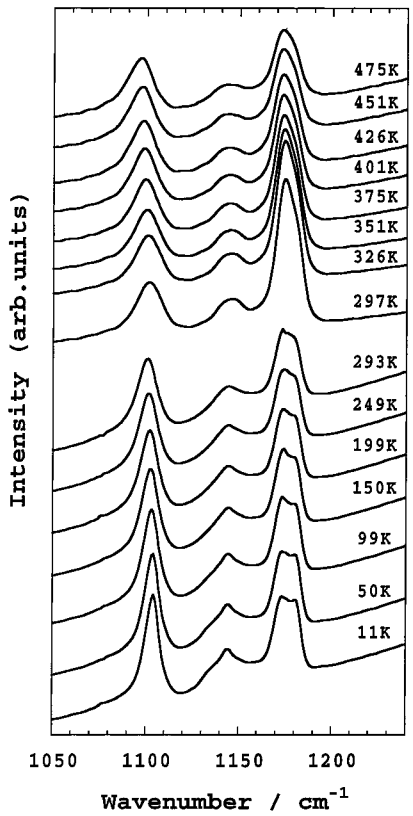

Figure 12. Temperature dependence of the IR absorption spectra of the C═S stretching mode in the *dta* ligands of $Pt_2(dta)_4I$.

T_{M-S}, which is the first example of a valence transition in MX or MMX chains. So one of modes (2)−(4) can be responsible for the semiconducting trapped-valence state. As discussed above, the semiconducting state is a Mott−Hubbard insulator. Accordingly, mode (3) is more favorable for the semiconducting state.

8. Alternate Charge Ordering. Judging only from IR study, there are three possible charge-ordering modes of (2) − (4) for the semiconducting phase below T_{M-S}, which was confirmed to be a trapped-valence state of Pt^{2+} and Pt^{3+}. Comparatively, modes (2) and (3) have only one chemically distinct bridging iodine, while mode (4) has two including both $Pt^{2+}-I-Pt^{2+}$ and $Pt^{3+}-I-Pt^{3+}$ bridges. To investigate the low-temperature charge-ordering mode, ^{129}I Mössbauer spectroscopic study was carried out. Unfortunately, experimental conditions of the 27.7 keV ^{129}I γ-ray resonance are limited to the research reactor due to an inconveniently short half-life, and to the low temperatures below 100 K, due to a not so good recoil-free fraction. However, there are lots of advantages of ^{129}I Mössbauer resonance which is very sensitive to the oxidation state and the chemical environment, and the iodine compounds show a wide variation in quadrupole splitting and isomer shift.[35]

The observed ^{129}I Mössbauer data, isomer shift (IS), nuclear quadrupole coupling constant (QCC), half-width (Γ), the intensity ratios of line2/line8 and line7/line 8 ($I_{2/8}$, $I_{7/8}$), the asymmetry parameter (η), the number of *p*-hole (h_p), the *p*-electron imbalance (U_p), and the relative intensity for $Pt_2(dta)_4I$ both at 16 and 80 K are given in Table 3. All IS values here are referenced to Mg_3TeO_6. To refer these isomer shifts to iodine in ZnTe, 3.49 (mm/s) have to be subtracted from the tabulated values. The half-life time of the excited state is rather long (16.8 ns), which gives well-resolved spectra with small natural line widths. The nuclear spin states of excited and ground states are $^5/_2$ and $^7/_2$, respectively, so that the quadrupole-split spectra consist of a minimum of eight lines.

Table 3. ^{129}I Mössbauer Data for $Pt_2(dta)_4I$ at 16 and 80 K

	IS[a]/mm·s^{-1}	e^2qQ/MHz	Γ/mm·s^{-1}	$I_{2/8}$	$I_{7/8}$	h	h_p	U_p	area
			16 K						
I_A	3.77	−1180	1.03	0.71	0.71	0	0.55	0.51	1.27
I_B	4.05	−1380	1.21	0.66	0.78	0	0.73	0.60	1.00
			80 K						
I_A	3.71	−1184	0.84	0.78	0.79	0	0.51	0.52	1.07
I_B	3.99	−1390	1.13	0.75	0.71	0	0.69	0.61	1.00

[a] Referenced to Mg_3TeO_6.

The observed ^{129}I Mössbauer spectra at 16 and 80 K are shown in Figure 13. A best fit is obtained with two octuplets for each spectra, which signifies the existence of two different iodine sites (I_A and I_B) in the MMX chain and favors mode (4): $\cdots Pt^{2+}-Pt^{3+}-I_A-Pt^{3+}-Pt^{2+}-I_B-Pt^{2+}-Pt^{3+}-I_A-Pt^{3+}-Pt^{2+}-I_B-Pt^{2+}-Pt^{3+}\cdots$

Assuming the charge-ordering mode (4), the intensity ratio of the two components should be primarily 1.0, the I_A/I_B compositional ratio in stoichiometric $Pt_2(dta)_4I$. However, the experimental ratios deviate from the expected ones. It is well-known that unequal intensities arise from differences in the recoil-free fractions f_A and f_B for the I_A and I_B sites in the chain.[36] The recoil-free fraction reflects the Debye−Waller factor of the iodine site: A larger Debye−Waller factor results in a larger recoil-free fraction. Since I_A anion coordinates to the higher-oxidized Pt^{3+} and I_B anion does to the lower-oxidized Pt^{2+}, the environment of the I_A is more rigid than that of the I_B. Accordingly, the inner octuplet with higher intensity is assigned to the bridging iodine (I_A) situated between Pt^{3+} and Pt^{3+}, and outer to that (I_B) between Pt^{2+} and Pt^{2+}. The spectrum at 16 K shows a larger difference in a recoil-free fraction between the two components than that at 80 K, which may be attributed to a gradual progress of lattice distortion, in lower temperature region, such a dimerization of two dimer units. Low-temperature X-ray single-crystal analysis will clarify the chain structure below 80 K, and is being planned.

Recently, supports for the charge-ordering mode (4) have been presented by experimental[37] and theoretical[38] works. Mitsumi et al.,[37a] has successfully synthesized several derivatives of $Pt_2(RCS_2)_4I$ (R = C_2H_5-, *n*-C_3H_7-, *n*-C_4H_9-, *n*-$C_5H_{11}-$). All of them are metallic or highly conductive and showing similar transitions to $Pt_2(dta)_4I$.[37b] From low-temperature X-ray analyses, it was revealed that $Pt_2(n\text{-}C_4H_9CS_2)_4I$ undergoes a phase transition around 200 K, below which well-formed satellite reflections at $\pm$ 0.5*b** from the layer of Bragg ones appears indicating a 3-D ordering of the structural modulation. This modulation was determined by the X-ray analysis including these satellite reflections to be like the alternate charge-ordering

(35) Parish, R. V. Mössbauer Spectroscopy Applied to Inorganic Chemistry. In *Mössbauer Spectroscopy with the Iodine Isotopes*; Long, G. J., Ed.; Plenum: New York, 1984; Vol. 2, p 391 and references therein.

(36) Viegers, T. P. A.; Trooster, J. M.; Brouten, P.; Rit, T. P. *J. Chem. Soc., Dalton Trans.* **1977**, 2074.

(37) (a) Mitsumi, M.; Toriumi, K., manuscript to be submitted. (b) Mitsumi, M.; Murase, T.; Matsumoto, M.; Ozawa, Y.; Toriumi, K.; Kobayashi, M.; Sonoyama, T.; Kitagawa, H.; Mitani, T. In Book of Abstracts. *XXXIII International Conference on Coordination Chemistry* (Florence) **1998**, p 385. (c) Mitsumi, M.; Ozawa, Y.; Toriumi, K., to be published.

(38) (a) Borshch, S. A.; Prassides, K.; Robert, V.; Solonenko, A. O. *J. Chem. Phys.* **1998**, *109*, 4562. (b) Robert, V.; Petit, S.; Borshch, S. A. submitted to *Inorg. Chem.* (c) Yamamoto, S. *Phys. Lett. A*, in press. (d) Kuwabara, M.; Yonemitsu, K. *Physica B*, manuscript submitted for publication. (e) Kuwabara, M.; Yonemitsu, K. *Mol. Cryst. Liq. Cryst*., in press.

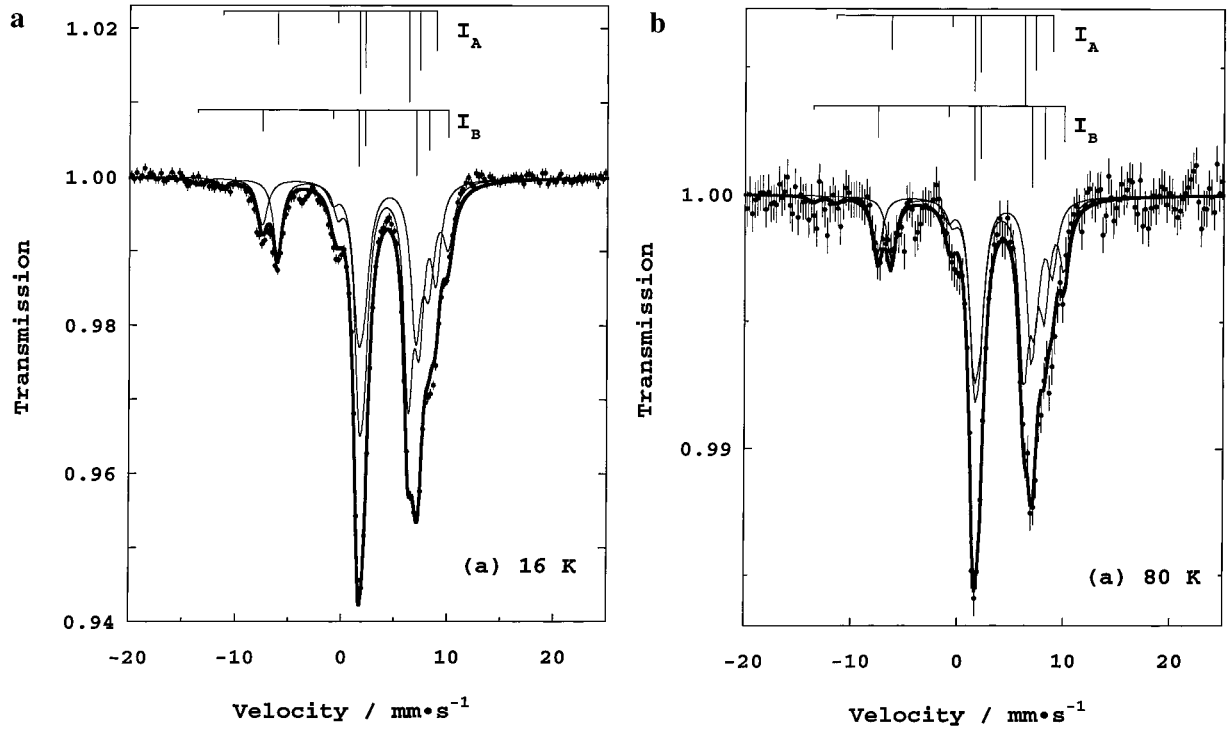

Figure 13. ^{129}I Mössbauer spectra of $Pt_2(dta)_4I$ at (a) 16 K, (b) 80 K.

mode (4).[37c] It should be also noted that Borshch et al.[38a,b] have performed several kinds of quantum-chemical calculations for an infinite $-M-M-X-$ chain and a four-nuclear cluster $X_1-M_1-M_2-X_2-M_3-M_4-X_3$; the ground-state charge-ordering mode was predicted to be alternate $-M^{2+}-M^{3+}-X-M^{3+}-M^{2+}-$ and it becomes more stable as the t_{intra} (t_{12} and t_{34}) is increased. On the other hand, Whangbo and Canadell have performed band calculations using extended Hückel methods for $Pt_2(dta)_4I$.[39] They have discussed the results on the basis of a possible Peierls instability of a metallic system and localized electronic states of an insulating system. The averaged-valence mode $-Pt^{2.5+}-Pt^{2.5+}-I-Pt^{2.5+}-Pt^{2.5+}-I-Pt^{2.5+}-Pt^{2.5+}-I-$ was predicted to be less stable $-I-Pt^{2+}-Pt^{2+}-I-Pt^{3+}-Pt^{3+}-I-Pt^{2+}-Pt^{2+}-I-Pt^{3+}-Pt^{3+}-I-$, which is partially inconsistent with our results. The reason is that they neglected the Coulomb repulsion parameters and did not discuss the alternate mode.

The alternate charge-ordering mode (4) is analogous to spin-Peierls state. If a spin-Peierls transition occurs, the spin susceptibility should be activated below the transition because of the freeze of spin degree of freedom. As shown in Figure 11, however, the spin degree of freedom survives down to 2 K, which is consistent with the preliminary solid-state ^{1}H NMR results.[33] If the alternate mode were strongly fluctuating Peierls-Hubbard state and not long-range ordered, the spin degree of freedom might not be frozen. It is a puzzle requiring further research.

The relation between the Mössbauer parameters and the valence-shell configuration of the iodine atom has been discussed many times.[35] The isomer shift (IS) is given by

$$\mathrm{IS} = C\Delta\langle R^2\rangle\rho(0) \qquad (3)$$

where C is constant containing nuclear parameters (>0), $\Delta\langle R^2\rangle$ is the change in the square of the nuclear radius between the excited and ground states, which has been estimated as $+19.5 \times 10^3$ fm^2 for ^{129}I, and $\Delta\rho(0)$ is the difference between the contact densities of the source and the absorber. For ^{129}I, therefore, a positive shift of IS indicates an increase in the electron density at the nucleus, $\rho(0)$. The iodine atom has a larger IS value of the order of $I^{-I} < I^0 < I^{+I}$ because of a decrease in the occupation of p orbitals in that order, resulting from screening of the valence and core s orbitals from the nucleus. The I^{+VII}, on the contrary, has a small value because of a direct decrease of the s-electron population in the valence shell. Especially in the case of the iodide ion which has a $5s^2$-$5p^6$ configuration, the IS value is well-known to be given by the following empirical equation:[35]

$$\mathrm{IS} = -9.2h_s + 1.5h_p - 0.54 \qquad (4)$$

where the IS values (mm/s) are referenced to ZnTe, and h_s and h_p are the fractional numbers of electrons missing from the full s and p shells. From this equation, the oxidation states of I_A and I_B can be estimated to be -0.45 and -0.27, respectively. Two important factors need to be considered for the charge distribution of iodine ions in the MMX chain. One is the covalence effect in $-Pt-I-Pt-$ bonds. The iodide ion which coordinates to the higher oxidized Pt^{3+} ions would be higher oxidation state than that to Pt^{2+} ions because of a larger iodine-to-platinum electron σ donation. The other is the Coulomb interaction between Pt^{2+} or Pt^{3+} and I^- ions. The iodide anion which is situated between Pt^{3+} cations would prefer lower oxidation state than that between Pt^{2+} ones. Accordingly, it is strongly suggested that the 1-D charge-ordering state of this MMX chain is governed mainly by the crystal field.

The QCC, on the other hand, is a direct measure of the electric field gradient (EFG) at the iodine nucleus.

$$\mathrm{QCC} = e^2qQ \qquad (5)$$

where e is the charge on the proton ($e > 0$), Q is the nuclear quadrupole moment (negative both for excited and ground states of ^{129}I), and EFG is often designated as eq (principal (z)

(39) Whangbo, M.-H.; Canadell, E. *Inorg. Chem.* **1986**, *25*, 1727.

component of EFG). The concentration of negative charge on the *xy* plane makes the EFG positive (the QCC is negative, since eQ is negative for ^{129}I), and that on the *z* axis does it negative (the QCC is positive). Most of the iodine (−I), iodine (0), and iodine (+I) compounds have negative QCC values, since they take electronic configurations from the closed-shell iodide ion, $5s^25p^6$, to a neutral iodine atom of I_2, $5s^25p^5$, toward the iodine-(+I) cation, $5s^25p^4$, and electron density is steadily lost from $5p_z$ orbital along the series. Therefore, an IS-QCC linear correlation is well-known in this series. Both of I_A and I_B sites in $Pt_2(dta)_4I$ also show the negative QCC values and its parameters follow the IS-QCC correlation. The site of I_B, which is situated between Pt^{2+} ions, shows a larger absolute value of QCC than that of I_A between Pt^{3+} ions. The following treatment is also well-known for NQR data,[35]

$$U_p = h_z - (h_x + h_y)/2 \quad (6)$$

$$= -e^2qQ^{127}h^{-1}/(2293\ \text{MHz}) \quad (7)$$

where U_p is the difference between the populations of the iodine $5p_z$ orbital and the $5p_x$ and $5p_y$ orbitals, and is sometimes referred to as the p-electron imbalance. The U_p values are estimated to be 0.6 and 0.51 for I_A and I_B, respectively. These results mentioned above indicate that the electron density of $5p_z$ orbital at I_B is smaller than that at I_A, which is consistent with the fact that I_B is more oxidized from −I toward 0 than I_A. It is noted that according to our preliminary measurement for $Ni_2(dta)_4I$, only one component of iodine was observed at 16 K, which implies a Mott−Hubarrd insulating state of mode (1). From the present Mössbauer spectroscopic study, it can be concluded that the charge-ordering mode (4) should be responsible for the insulating phase below 80 K.

Concluding Remarks

In this work, we have demonstrated that the present MMX chain is a unique 1-D spin-charge-lattice coupled system. The MMX chain $Pt_2(dta)_4I$ exhibits metallic conduction between 300 and 365 K, which is the first example of a metallic halogen-bridged 1-D transition-metal complex. This metallic state exhibits averaged valency of $-I-Pt^{2.5+}-Pt^{2.5+}-I-Pt^{2.5+}-Pt^{2.5+}-$, as well as the high-temperature metallic disordered phase. The metal−insulator transition occurs at 300 K, originating from the Mott transition with 1-D charge ordering of $-I-Pt^{2+}-Pt^{3+}-I-Pt^{2+}-Pt^{3+}$-. The valence transition at T_{M-S} is considered to be due to valence instability of $Pt^{2.5+}$, arising from an effective intradimer and interdimer Coulomb interactions. Below 80 K, it is strongly suggested that an alternate charge ordering of $-I-Pt^{2+}-Pt^{3+}-I-Pt^{3+}-Pt^{2+}-$ occurs, accompanied by the dimerization of two dimers. Although this alternate mode is analogous to spin-Peierls state, the spin degree of freedom survives down to 2 K. In the present 1-D highly conductive material, spin fluctuations coupled with charge and lattice degrees of freedom is considered to play an important role and further investigations are in progress to explain the alternate charge-ordering state.

Experimental Section

Syntheses. The title complex was prepared by the method previously reported.[13a] The single crystals were grown in toluene solution which contained $Pt_2(dta)_4$ and I_2. The quality of obtained single crystals were confirmed by X-ray single-crystal analysis, elemental analysis, and IR spectroscopy.

X-ray Photoelectron Spectroscopy. The X-ray photoelectron spectroscopy (XPS) measurements were carried out on a VG ESCA MKII electron spectrometer at the Institute for Molecular Science, the source vacuum being $< 1 \times 10^{-8}$ mbar, with a Mg−Kα X-ray source (1253.6 eV) in the temperature range of 150−300 K. The pass-energy of a hemisphere analyzer was constant (20 eV). Binding energies were measured relative to the C 1*s* peak due to hydrocarbon contamination from the diffusion pump, which built up slowly on the surface under these operating conditions. The absolute binding energy (284.4 eV) of the contaminant C 1*s* peak was confirmed by measuring its energy on the surface of silver foil (Ag $3d_{5/2} = 367.9$ eV)[19] after the Ar^+ ion sputtering to the foil. Absence of X-ray beam effects was checked by the X-ray power dependence of XPS spectra.

Electrical Conductivity Measurements. The dc electrical-conductivity measurements were performed along the chain axis (||*b*) between 50 and 380 K on several single crystals with the excitation of 0.1−1μA by a conventional four-probe method using gold paint and gold wire (20 μm ϕ). The temperature was measured with a calibrated Pt-(Co) resistance thermometer (Chino R800−6) in the temperature range of $150 < T < 335$ K and silicon diode sensor (LakeShore DT-470) in the temperature range of $50 < T < 380$ K, both placed near the sample. The cooling or heating rate was about 0.3 K/min. The reproducibility of the conductivity behavior was checked for different crystals.

Thermoelectric Power Measurements. The thermoelectric power measurement was made by a dynamical differential method. The single crystal of $Pt_2(dta)_4I$ was placed, via two very short gold wires (20 μm ϕ) used as a damper, on the tip of two sets of spot welded fine Au-(Fe)-chromel thermocouples (76 μm ϕ) insulated with poly(tetrafluoroethylene) and was gold painted. A small auxiliary heater was below one of the thermocouples. The temperature gradient across the needle crystal was increased by the heater up to ~0.5 K and simultaneously measured by the thermocouples connected to separate nanovoltmeters (Keithley 182). The experimental calibration of the chromel wire used as a working thermocouple was proceeded by a pure lead sample (>99.999%). The absolute thermoelectric power was then calculated by correcting for that of the calibrated chromel. The temperature was controlled by LakeShore Model 330 and measured with a calibrated silicon diode sensor (LakeShore DT-470) placed near the sample.

Polarized Reflectance Spectroscopy. Polarized reflectance measurements of single crystals were made at rt in the energy range 0.1 eV − 3.5 eV with a microscopic system (Spectra Tech, IR−Plan) with Nicolet FTIR 710, MAGNA-IR 760, and Jasco CT-25 spectrometers. The detectors of photomultiplier tubes, PbS, Ge, and MCT were used.

Polarized Raman Spectroscopy. Polarized Raman spectra of single crystals were recorded with a Jasco NR-1800 subtractive-dispersion triple (filter single) polychromator using a microscope. A Spectra-Physics model 2017 Ar^+ laser provided the exciting line (514.5 nm). Detection of the scattered radiation was by a cooled Photometrics CC200 CCD camera system with operating temperature of 153 K. Laser power at the crystals was held to <1mW to avoid laser damage to samples. To reduce stray light from Rayleigh scattering and enable low-frequency Raman spectroscopy down to 20 cm^{-1}, the positions of double subtractive premonochromator and third monochromator were shifted to each other by 50 cm^{-1} and the Rayleigh light was cut by a slit between the first and second monochromators. Wavenumber calibration was effected by reference to the Raman spectrum of indene, the emission spectrum of Ne lamp, and plasma lines of Ar^+ laser. The typical dimension of flat needlelike crystal was ~2 × 0.4 × 0.1 mm. The $Z(YY)\bar{Z}$ and $Z(XX)\bar{Z}$ components of the scattered radiation were used, where X||*c**, Y||*b**, Z||*a**−*c** (~*a*), and the 1-D chain||*b** (=*b*).

IR Spectroscopy. For IR absorption measurements, powdered samples ground down from single crystals were diluted with KBr and then the mixtures were processed into pellets under pressure (~6 kbar) and vacuous condition. IR spectra were measured in the temperature region of 11−475 K by a Nicolet FTIR 800 spectrometer with a DAIKIN CryoKelvin 202CL cryostat that possesses KRS-5 optical windows. IR detectors of TGS and MCT were used.

Magnetic Susceptibility Measurements. The magnetic susceptibility measurement of a polycrystalline sample was performed in the temperature range of 2−400 K using a Quantum Design MPMS-5 SQUID magnetometer. The total diamagnetic contributions of $Pt_2(dta)_4I$ were estimated as the sum of the measured value for $Pt_2(dta)_4$ and half the reference value of I_2.

^{129}I Mössbauer spectroscopy. Mössbauer spectroscopic measurements of the 27.7keV transition in ^{129}I were carried out with both source and absorber cooled to 16 K by using a constant-acceleration spectrometer with a NaI(Tl) scintillation counter and a DAIKIN CryoKelvin closed-cycle refrigerator system employing helium gas as a working medium. The data were stored in a microcomputerized 512 multichannel analyzer. A ^{129}Te source was obtained by neutron irradiation of enriched $Mg_3{}^{128}TeO_6$ due to the nuclear reaction ^{128}Te-$[n,\gamma]^{129m}$Te in the Kyoto University Reactor (KUR). The half-life time of the precursor ^{129m}Te isotope is 33 days. The velocity scale was calibrated by taking spectra of body-centered cubic iron against a ^{57}Co source, both at rt. The observed spectra were analyzed by use of a computer program including folding and least-squares fitting with Lorentzian lines. The sample for Mössbauer spectroscopy with iodine was synthesized as a black powder using radioactive isotope ^{129}I (19.7 mg) in a draft chamber of KUR by the following chemical reactions;[40]

$$2Na^{129}I + Na_2SO_3 + 2H_2O_2 + H_2SO_4 \rightarrow 2Na_2SO_4 + 3H_2O + {}^{129}I_2$$

$$2Pt_2(dta)_4 + {}^{129}I_2 \rightarrow 2Pt_2(dta)_4{}^{129}I$$

Acknowledgment. The authors wish to thank Professor P. Day for his continuous encouragement. We also thank Professors M. Yamashita, K. Toriumi, R. Ikeda, Y. Iwasa, K. Prassides, S. A. Borshch, V. Robert, K. Kanoda, K. Yonemitsu, S. Kuroda, M. Yamamoto, and M. Sorai for stimulating discussions. Thanks are also due to the Research Center for Molecular Materials, the Institute for Molecular Science, for assistance in obtaining the XPS spectra. This work was partly supported by Grant-in-Aid Scientific Researches No. 09640686 and No. 401 of Priority Areas (Metal-Assembled Complexes) from the Ministry of Education, Science, Sports and Culture, Japan, and by the Murata Science Foundation.

JA9915910

(40) Kojima, N.; Sakai, H.; Seto, M.; Kitao, S.; Maeda, Y. In Conference Proceedings; *International Conference on the Applications of the Mössbauer Effect*, SIF, Bologna, 1996; Vol. 50, p 47.